

# Probing low-mass WIMP candidates of dark matter with tetrafluoroethane superheated liquid detectors

Susnata Seth<sup>\*,†</sup> Sunita Sahoo<sup>1,2,‡</sup> Pijushpani Bhattacharjee<sup>1,§</sup> and Mala Das<sup>1,2,¶</sup>

<sup>1</sup>*Astroparticle Physics & Cosmology Division,*

*Saha Institute of Nuclear Physics, Kolkata 700064, India*

<sup>2</sup>*Homi Bhabha National Institute, Training School Complex,*

*Anushakti Nagar, Mumbai 400094, India*

## Abstract

Probing low mass (sub-GeV – few GeV) Weakly Interacting Massive Particle (WIMP) candidates of dark matter through WIMP-induced nuclear recoils in direct detection experiments requires use of detector materials consisting of low mass target nuclei and low threshold energy. Here we explore the potential of superheated liquid detectors (SLD) with a hydrogen containing liquid, namely, tetrafluoroethane ( $\text{C}_2\text{H}_2\text{F}_4$ ) (b.p.  $-26.3^\circ\text{C}$ ), as the target material for probing low mass WIMPs. It is found that few-keV level recoil energy thresholds possible for bubble nucleation by WIMP-induced  $^{12}\text{C}$  and  $^{19}\text{F}$  recoils in  $\text{C}_2\text{H}_2\text{F}_4$  SLDs operated at atmospheric pressure and gamma-ray insensitive temperatures of  $T \lesssim 35^\circ\text{C}$  have the potential to allow WIMPs in the few-GeV mass range to be probed at a WIMP-nucleon spin-independent cross section sensitivity levels (90% C.L.) better than  $4.6 \times 10^{-5}$  pb at WIMP masses down to  $\sim 4$  GeV with a total exposure of  $\sim 1000$  kg.day, provided that the “thermodynamic efficiency”  $\eta_T$  that determines the bubble nucleation thresholds for the recoiling nuclei in  $\text{C}_2\text{H}_2\text{F}_4$  is  $\sim 50\%$  or higher. Sensitivity to sub-GeV WIMP masses generally requires the detector to be sensitive to the WIMP-induced  $^1\text{H}$  recoils, which in turn requires the detector to be operated at temperatures  $T \gtrsim 50^\circ\text{C}$  and  $\eta_T$  close to 100%. At such relatively high temperatures (at atmospheric pressure), however, the detector would be sensitive to background gamma rays.

---

\* Presently at Bose Institute, EN-80, Sector V, Bidhannagar, Kolkata 700091, India.

†Electronic address: susnata.seth@gmail.com

‡Electronic address: sunita.sahoo@saha.ac.in

§Electronic address: pijush.bhattacharjee@saha.ac.in

¶Electronic address: mala.das@saha.ac.in

## I. INTRODUCTION

Weakly Interacting Massive Particles (WIMPs) [1–3] predicted in many theories beyond the Standard Model of particle physics, with masses of a few GeV to a few hundred TeV<sup>1</sup> are one of the major candidates for the constituents of the Dark Matter (DM), an unknown form of non-luminous matter that constitutes about 85% of the total gravitating mass and about 27% of the total mass-energy budget of the Universe; see, e.g., Ref. [4] for a recent review. Following the early suggestion [5] that nuclear recoil events due to elastic scattering of the Galactic WIMPs off nuclei of suitably chosen detector materials may be detectable, a large number of experiments worldwide have been engaged for the past three decades or so in efforts to detect the WIMPs employing various detection techniques. The kinetic energy of a recoiling nucleus due to WIMP-nucleus elastic scattering, which can be anywhere in the range of a few keV to few hundreds of keV depending on the WIMP and target nucleus masses, would be dissipated in the detector medium providing signals in the form of bolometric heat, lattice vibration (phonon), ionization, scintillation light, and so on, depending on the detector medium [6, 7]. The DAMA/LIBRA experiment [8–10] has been consistently reporting, for about a decade now, a statistically significant detection of an annual modulation signal in their event rate, which they attribute to WIMPs, the annual modulation being attributed to Earth’s motion around the Sun [11, 12]. However, the DAMA/LIBRA results are difficult to reconcile with the null results from a number of other experiments which have set rather stringent upper limits on the WIMP-nucleon interaction strength [13–18].

Most of the currently running experiments are designed to be optimally sensitive to WIMPs of mass  $\gtrsim 10$  GeV. In view of the null results from these experiments, recently there has been much interest in experiments designed to be specifically sensitive to relatively lower mass ( $< 10$  GeV) WIMPs; see, for example, Refs. [13, 18–21]. Sensitivity to low mass WIMPs generally require low (sub-keV) recoil energy threshold and detector materials containing low mass nuclei.

In this paper we study the possibility of probing low mass (sub-GeV – few GeV) WIMPs with a detector material containing hydrogen, the lowest-mass target nucleus possible.

---

<sup>1</sup> We use units with  $c = 1$  throughout this paper.

Specifically, we consider the superheated liquid tetrafluoroethane ( $\text{Z}h2f4$ ), a low-cost, commercially available, environment friendly (chlorine free) refrigerant liquid (b.p.  $-26.3^\circ\text{C}$ ) as the target detector material.

Superheated liquid based detectors with liquids such as  $\text{C}_3\text{F}_8$ ,  $\text{CF}_3\text{I}$ ,  $\text{C}_4\text{F}_{10}$ ,  $\text{C}_2\text{ClF}_5$ , and so on have been extensively used for WIMP direct detection experiments [14, 22–25]. The superheated liquid state being a metastable state of the liquid [26], the energy deposited by a recoiling nucleus arising from WIMP-nucleus scattering in the liquid can induce a phase transition from the superheated liquid state to vapor state if the deposited energy exceeds a certain critical energy that depends on the temperature and pressure of the liquid. The acoustic pulse generated during such a phase transition provides the signal which can be detected by acoustic sensors. The phase transition from the superheated liquid state to the vapor state occurs through nucleation of vapor bubbles of certain critical size. Since bubble nucleation can occur only if the energy deposition is above a certain critical amount, this makes such detectors act as threshold detectors, with the threshold energy controlled by the temperature and pressure of the liquid. A major advantage of superheated liquid detectors is their operability at room temperatures as opposed to cryogenic temperatures required for most other kinds of WIMP search detectors currently under operation. Moreover, by controlling the threshold energy of the detector with judicious choice of the operating temperature and pressure, the detector can be made insensitive to certain kinds of particles, for example, beta particles and gamma-rays, which constitute the main sources of background for most WIMP search experiments.

Gamma ray and neutron sensitivities of superheated liquid detectors with  $\text{Z}h2f4$  as the active liquid have been studied earlier in various contexts including neutron dosimetry and spectrometry; see, e.g., [27–30]. Recently, the PICO collaboration has started exploring the possibility of using  $\text{Z}h2f4$  for low-mass WIMP detection [31]. Work has also been done studying bubble nucleation due to proton recoils in  $\text{Z}h2f4$  using 22.8 keV neutrons from a  $^{124}\text{SbBe}$  source [32]. Our aim in this paper is to present a theoretical study of the response of superheated liquid  $\text{Z}h2f4$  detectors to low-mass WIMPs within the general context of Seitz’s [33] phenomenological theory of bubble nucleation in superheated liquids. In particular, we theoretically study the behavior of the bubble nucleation threshold energies of the WIMP-induced recoiling hydrogen ( $^1\text{H}$ ), carbon ( $^{12}\text{C}$ ) and fluorine ( $^{19}\text{F}$ ) nuclei in  $\text{Z}h2f4$  at various temperatures and the corresponding lowest WIMP mass that can be probed with

$\text{C}_2\text{F}_6$  detectors.

Below, in section II we briefly review the basic working principle of superheated liquid detectors (SLD) and discuss the method we follow to calculate the bubble nucleation threshold energies of various particles moving through the liquid. In section III we discuss the response of SLD to spin-independent elastic scattering of the WIMPs constituting the DM halo of our Galaxy, focusing on the lowest WIMP mass to which the SLD can be sensitive. Section IV presents our results for the bubble nucleation threshold energies of recoiling hydrogen ( $^1\text{H}$ ), carbon ( $^{12}\text{C}$ ) and fluorine ( $^{19}\text{F}$ ) nuclei in superheated liquid  $\text{C}_2\text{F}_6$  and the corresponding lowest WIMP mass that can be probed with  $\text{C}_2\text{F}_6$  SLD as a function of temperature. Finally, section V summarizes our main results and conclusions.

## II. SUPERHEATED LIQUID DETECTORS: BASIC PRINCIPLES

A Superheated Liquid Detector (SLD) works on the basic principle that localized energy deposition during the passage of an energetic particle through the liquid can cause a phase transition from the liquid state to the vapor phase. According to Seitz’s phenomenological “heat spike” theory [33], the phase transition occurs through nucleation of vapor bubbles of radii larger than a critical radius ( $R_c$ ) due to localized deposition of energy by the particle within the superheated liquid. The bubbles of radii smaller than  $R_c$  collapse back to the liquid state while those with radii larger than  $R_c$  expand and grow to visible size through evaporation of the liquid. The expansion of the vapor bubble is accompanied by production of an acoustic pulse which acts as the signal carrying information about the energy deposited in the liquid due to the passage of the particle.

At a given temperature and pressure, the critical radius ( $R_c$ ) is given by [33]

$$R_c = \frac{2\sigma(T)}{(P_v - P_l)}, \quad (1)$$

where  $\sigma(T)$  is the liquid-vapor interfacial tension at temperature  $T$ ,  $P_v(T)$  is the vapor pressure and  $P_l(T)$  is the pressure of the liquid. To form a bubble of critical radius the particle must have an energy<sup>2</sup>,  $E$ , equal to or greater than a certain threshold energy,  $E_{\text{th}}$  such that the energy deposited by the particle,  $E_{\text{dep}}^{2R_c}$ , over a path segment of length  $2R_c$  (the

---

<sup>2</sup> Throughout this paper, we shall be concerned with particles of non-relativistic speeds, and hence by energy of a particle we shall mean its non-relativistic kinetic energy.

“critical diameter”) along the particle’s track in the liquid satisfies the condition

$$E_{\text{dep}}^{2R_c}(E = E_{\text{th}}) \equiv \int_0^{2R_c} \left( \frac{dE}{dx} \right) dx = E_c/\eta_T, \quad (2)$$

where  $\frac{dE}{dx}$  is the stopping power of the liquid for the particle under consideration,  $\eta_T \leq 1$  is the “thermodynamic efficiency” [34] and  $E_c$  is the minimum (“critical”) energy required for bubble nucleation, which is given by [33, 35]

$$E_c = 4\pi R_c^2 \left( \sigma - T \frac{\partial \sigma}{\partial T} \right) + \frac{4\pi}{3} R_c^3 \rho_v (h_v - h_l) - \frac{4\pi}{3} R_c^3 (P_v - P_l), \quad (3)$$

where  $\rho_v(T)$  is the vapor density, and  $h_v(T)$ ,  $h_l(T)$  are the specific enthalpies of the vapor bubble and liquid, respectively. Equation (2) also serves to define the thermodynamic efficiency  $\eta_T$  as a measure of the fraction of the energy deposited by the particle within  $2R_c$  that goes into nucleation of a bubble of critical radius  $R_c$ , and is a characteristic of the superheated liquid under consideration.

If at any given temperature and pressure the mean range<sup>3</sup>,  $R$ , of the particle at energy  $E = E_c/\eta_T$  satisfies  $R(E = E_c/\eta_T) \leq 2R_c$ , then we have  $E_{\text{th}} = E_c/\eta_T$ . On the other hand, if  $R(E_c/\eta_T) > 2R_c$ , then  $E_{\text{th}}$  will be larger than  $E_c/\eta_T$  and is determined by equation (2). Also, since at a given pressure the critical energy  $E_c$  decreases with increasing temperature (see Table I below), the energy threshold  $E_{\text{th}}$  translates to a temperature threshold,  $T_{\text{th}}$ , for bubble nucleation, with lower  $E_{\text{th}}$  corresponding to higher  $T_{\text{th}}$  and vice versa.

Clearly, the threshold energy for bubble nucleation depends on the value of the thermodynamic efficiency  $\eta_T$ , which is *a priori* unknown, and can only be determined through experiment. The Seitz theory [33] generally assumes  $\eta_T = 1$ , in which case  $E_{\text{th}} \geq E_c$ . For this reason, the energy  $E_c$  is often referred to as the “Seitz threshold”. Recent results from the PICO experiment [35, 36] seem to suggest that the actual bubble nucleation threshold energy  $E_{\text{th}}$  of different nuclei can in fact be significantly larger than the Seitz threshold  $E_c$  (as defined by equation (3)), with the lighter nuclei generally having larger values of the ratio  $E_{\text{th}}/E_c$ . From Figure 3 of Ref. [36] we see that, in terms of our parameter  $\eta_T$ , the  $1\sigma$  bands of the experimental values of  $E_{\text{th}}/E_c$  for bubble nucleation thresholds of  $^{12}\text{C}$  and  $^{19}\text{F}$  recoils in  $\text{C}_3\text{F}_8$  would correspond to values of  $\eta_T$  ( $= E_c/E_{\text{th}}$  in these cases — see the

---

<sup>3</sup> The range is defined as the average distance over which the particle loses all its kinetic energy and comes to a stop in the liquid.

discussions in the previous paragraph) roughly in the range  $\sim 0.3 - 0.9$ . Taking cues from these results, we may expect similar values of the parameter  $\eta_T$  to be applicable in the case of  $\text{ZnF}_2$  too, at least for  $^{12}\text{C}$  and  $^{19}\text{F}$ , since both these nuclei behave roughly similarly in the two liquids as far as their energy deposits (determined by the ratio of their range  $R$  to the critical radius  $R_c$  in the liquid under consideration) are concerned. Based on the above considerations, in absence of any direct experimental results on the threshold energies of individual nuclei in the case of  $\text{ZnF}_2$ , in this paper we shall do the calculations and show the results for the event rates and WIMP-mass sensitivities for  $\text{ZnF}_2$  for two different values of  $\eta_T$ , namely, 50% and 100%, for illustration.

The threshold energy  $E_{\text{th}}$  marks the *onset* of bubble nucleation, with no bubble nucleation occurring below this energy. However, in reality, the process of bubble nucleation being a probabilistic one, the efficiency of bubble nucleation may not be 100% at the energy  $E_{\text{th}}$  itself, but may reach full efficiency only at a somewhat higher value of energy, as seen in experiments [35, 36]. The nucleation efficiency curves, i.e., the bubble nucleation efficiency as a function of the ion's recoil energy, of individual ions in  $\text{ZnF}_2$  are not known. However, the PICO experiment [36] has determined, albeit with large uncertainties, the bubble nucleation efficiency curves of  $^{12}\text{C}$  and  $^{19}\text{F}$  recoils in  $\text{C}_3\text{F}_8$ . To make progress, based on the discussions in the previous paragraph, below we shall use these efficiency curves for  $^{12}\text{C}$  and  $^{19}\text{F}$  in  $\text{C}_3\text{F}_8$ , appropriately scaled to their respective threshold energies in  $\text{ZnF}_2$ , for our calculations of the expected event rates and WIMP mass sensitivities of  $\text{ZnF}_2$  due to  $^{12}\text{C}$  and  $^{19}\text{F}$  recoils. For  $^1\text{H}$  recoils, in absence of any direct experimental results on their efficiency curves, we shall assume 100% bubble nucleation efficiency at threshold as in previous studies [32].

### III. RESPONSE OF SUPERHEATED LIQUID DETECTOR TO WIMPS

In a direct detection experiment for DM search, the detector looks for signatures of nuclear recoils produced by scattering of the WIMPs off the nuclei of the detector material. The recoil energy of the nucleus,  $E_R$ , due to WIMP-nucleus elastic scattering is given by

$$E_R = \frac{\mu_{\chi A}^2 v^2}{m_A} (1 - \cos \theta), \quad (4)$$

where  $v = |\mathbf{v}|$  is the speed of the WIMP relative to the target nucleus at rest on Earth,  $\theta$  is the WIMP scattering angle in the WIMP-nucleus center-of-mass system,  $m_\chi$  and  $m_A$  are

the WIMP and target nucleus masses, respectively, and  $\mu_{\chi A} = \frac{m_\chi m_A}{m_\chi + m_A}$  is the WIMP-nucleus reduced mass. The minimum WIMP speed,  $v_{\min}$ , that can produce a recoil nucleus with energy  $E_R$  is given by

$$v_{\min} = \left( \frac{E_R m_A}{2\mu_{\chi A}^2} \right)^{1/2}. \quad (5)$$

The differential recoil rate,  $d\mathcal{R}/dE_R$ , i.e., the number of nuclear recoil events per unit time per unit detector mass per unit recoil energy can be written as [2, 37]

$$\frac{d\mathcal{R}}{dE_R} = \frac{\sigma_{\chi A}(0) \rho_{\text{DM}}}{2m_\chi \mu_{\chi A}^2} F^2(q) \int_{v_{\min}(E_R)} d^3v \frac{f(\mathbf{v}, t)}{v}, \quad (6)$$

where  $\sigma_{\chi A}(0)$  is the ‘zero momentum transfer’ WIMP-nucleus cross-section,  $\rho_{\text{DM}} \approx 0.3 \text{ GeV}/\text{cm}^3$  is the local mass density of DM [38],  $f(\mathbf{v}, t)$  is the WIMP velocity distribution in the Earth’s rest frame, the time dependence being due to Earth’s revolution around the Sun [11, 12], and  $F(q)$  (with  $F(0) = 1$ ) is the nuclear form factor with  $q = (2m_A E_R)^{1/2}$  the momentum transfer from the WIMP to the nucleus.

For the WIMPs’ velocity distribution, we shall assume the standard halo model (SHM) in which the DM halo of the Galaxy is described by an isothermal sphere [39] with an isotropic velocity distribution of the Maxwell-Boltzmann form in the Galactic rest frame truncated at the local Galactic escape speed  $v_{\text{esc}}$  and Galilean boosted to the Earth’s frame (see, e.g., [12, 37]):

$$f(\mathbf{v}, t) = \frac{1}{\kappa} \frac{1}{(\pi v_0^2)^{3/2}} \exp \left\{ -\frac{(\mathbf{v} + \mathbf{v}_E)^2}{v_0^2} \right\} \Theta(v_{\text{esc}} - |\mathbf{v} + \mathbf{v}_E|), \quad (7)$$

where  $v_0 = (\frac{2}{3}\langle v^2 \rangle)^{1/2} \simeq 220 \text{ km s}^{-1}$  is the characteristic (most probable) speed of the DM particles in the Galaxy,  $\mathbf{v}_E(t)$  is the velocity of the Earth with respect to the Galactic rest frame,

$$\kappa = \text{erf} \left( \frac{v_{\text{esc}}}{v_0} \right) - \frac{2}{\sqrt{\pi}} \frac{v_{\text{esc}}}{v_0} \exp \left( -\frac{v_{\text{esc}}^2}{v_0^2} \right) \quad (8)$$

is a normalization constant, and  $\Theta(x)$  is the unit step function. The exact value of  $v_{\text{esc}}$  is not known with certainty. Values in the range from 498 to 608  $\text{km s}^{-1}$  (90% C.L.) are quoted in literature, with a median value of  $\sim 540 \text{ km s}^{-1}$  [40], which we shall use in this paper for all numerical estimates.

In this paper we shall not consider the (small) annual modulation of the recoil rate (6) due to Earth’s revolution around the Sun [11, 12], and consider only the annual average value of the recoil rate with the average value of  $v_E = |\mathbf{v}_E| \simeq 232 \text{ km s}^{-1}$ .

With the WIMP speed distribution given by equation (7), the differential recoil rate (equation (6)) for a detector consisting of nuclei of mass number  $A$  and atomic number  $Z$  can be written as [37]

$$\frac{d\mathcal{R}}{dE_R} = \kappa^{-1} \frac{\mathcal{R}_0}{rE_0} F^2(q) \left[ \frac{\sqrt{\pi}}{4} \frac{v_0}{v_E} \left\{ \operatorname{erf}\left(\frac{v_{\min} + v_E}{v_0}\right) - \operatorname{erf}\left(\frac{v_{\min} - v_E}{v_0}\right) \right\} - \exp\left(\frac{-v_{\text{esc}}^2}{v_0^2}\right) \right], \quad (9)$$

where  $\mathcal{R}_0 = \frac{2}{\sqrt{\pi}} \frac{N_0}{A} \frac{\rho_{\text{DM}}}{m_\chi} \sigma_{\chi A}(0) v_0$ ,  $N_0 = 6.022 \times 10^{26} \text{ kg}^{-1}$  is the Avogadro number,  $r = \frac{4m_A m_\chi}{(m_A + m_\chi)^2}$ , and  $E_0 = \frac{1}{2} m_\chi v_0^2$ . Note, in equation (9), the  $E_R$  dependence is contained in  $v_{\min}$  [see equation (5)] and the form factor  $F(q)$ . The latter can be taken to be of the form [37]

$$F(q) = 3 e^{-(qs)^2/2} \frac{\sin(qr_n) - qr_n \cos(qr_n)}{(qr_n)^3}, \quad (10)$$

where  $r_n$  is the effective nuclear radius given by  $r_n^2 = c^2 + \frac{7}{3}\pi^2 a^2 - 5s^2$  with  $c \simeq 1.23A^{1/3} - 0.60$  fm, and nuclear skin thickness parameters  $a \simeq 0.52$  fm and  $s \simeq 0.9$  fm.

In this paper, we shall restrict ourselves to the case of coherent, spin-independent (SI) WIMP-nucleus interaction. In this case, assuming isospin independent WIMP-nucleon coupling, the zero momentum WIMP-nucleus cross section  $\sigma_{\chi A}(0)$  can be written in terms of the SI WIMP-nucleon cross section,  $\sigma_{\chi n}^{\text{SI}}$ , as

$$\sigma_{\chi A}(0) = \sigma_{\chi A}^{\text{SI}}(0) = \sigma_{\chi n}^{\text{SI}} \frac{\left(1 + \frac{m_\chi}{m_n}\right)^2}{\left(1 + \frac{m_\chi}{m_A}\right)^2} A^2, \quad (11)$$

where  $m_n$  is the nucleon (neutron or proton) mass.

For a detector made of a compound target material consisting of different elements  $i$  of mass numbers  $A_i$  and nuclear masses  $m_{A_i}$ , as is the case in this paper, the differential recoil rate (per unit mass of the compound target material) is given by

$$\frac{d\mathcal{R}}{dE_R} = \sum_i \xi_i \left( \frac{d\mathcal{R}}{dE_R} \right)_i, \quad (12)$$

where  $\xi_i$  is the mass fraction of the target element  $i$  in the detector ( $\sum_i \xi_i = 1$ ), and the recoil rate  $(d\mathcal{R}/dE_R)_i$  for the element  $i$  is calculated from equation (9) with  $A$  replaced by  $A_i$  and  $m_A$  by  $m_{A_i}$  in all the relevant quantities.

The expected rate of events,  $\mathcal{R}_{\text{exp}}$ , i.e., number of events per unit mass of the compound target material per unit time, is then given by

$$\mathcal{R}_{\text{exp}} = \sum_i \mathcal{R}_{\text{exp}}^{(i)} = \sum_i \xi_i \int_{E_{\text{R,th}}^{(i)}}^{E_{\text{R,max}}^{(i)}} dE_{\text{R}} \epsilon_i(E_{\text{R}}) \left( \frac{d\mathcal{R}}{dE_{\text{R}}} \right)_i, \quad (13)$$

where  $\epsilon_i(E_{\text{R}})$  is the bubble nucleation efficiency and  $E_{\text{R,th}}^{(i)}$  is the recoil energy threshold for bubble nucleation by nuclei of element  $i$ , and

$$E_{\text{R,max}}^{(i)} = \frac{2m_{A_i}v_{\text{esc}}^2}{\left(1 + \frac{m_{A_i}}{m_{\chi}}\right)^2} \quad (14)$$

is the maximum recoil energy a nucleus of element  $i$  can receive due to scattering with a WIMP of mass  $m_{\chi}$ . Note that  $E_{\text{R,max}}^{(i)}$  decreases with decreasing value of  $m_{\chi}$ . Therefore, for a given target material element  $i$ , the condition  $E_{\text{R,max}}^{(i)} \geq E_{\text{R,th}}^{(i)}$  for bubble nucleation by a recoiling nucleus of target element  $i$  implies that the target element  $i$  is insensitive to WIMPs of masses below a certain lowest value,  $m_{\chi,\text{lowest}}^{(i)}$ , given by

$$m_{\chi,\text{lowest}}^{(i)} = m_{A_i} \left[ \left( \frac{2m_{A_i}v_{\text{esc}}^2}{E_{\text{R,th}}^{(i)}} \right)^{1/2} - 1 \right]^{-1}. \quad (15)$$

Note that, for a SLD, since  $E_{\text{R,th}}^{(i)}$  depends on the operating temperature and pressure of the SLD as discussed in section II above, the lowest WIMP mass  $m_{\chi,\text{lowest}}^{(i)}$  that can be probed with target element  $i$  also depends on the operating temperature and pressure of the SLD.

## IV. RESULTS AND DISCUSSION

### A. Threshold energies of recoiling $^1\text{H}$ , $^{12}\text{C}$ and $^{19}\text{F}$ nuclei for bubble nucleation in superheated liquid $\text{z}^2\text{f}_4$

As discussed in section II, to obtain the bubble nucleation threshold energy of a particular recoiling nucleus, we need to first compare the range of the nucleus at energy  $E_c/\eta_{\text{T}}$  for a given value of  $\eta_{\text{T}}$  with the critical diameter  $2R_c$  at the given operating temperature and pressure of the SLD. We calculate the critical radius  $R_c$  [equation (1)] and the critical energy  $E_c$  [equation (3)] using values of the thermodynamic quantities taken from the REFPROP database maintained by the National Institute of Standards and Technology [41]. The ranges of  $^1\text{H}$ ,  $^{12}\text{C}$  and  $^{19}\text{F}$  nuclei in superheated liquid  $\text{z}^2\text{f}_4$  are calculated using the ‘‘Stopping Range of Ions in Matter’’ (SRIM) software package [42]. For simplicity, all results shown below are for operating pressure fixed at 1 atm.

Operating Temperature ( $T$ ) (° C)	Critical Energy ( $E_c$ ) (keV)	Critical Radius ( $R_c$ ) (nm)	$2R_c$ (nm)	Range ( $E = E_c$ )		
				$^1\text{H}$ (nm)	$^{12}\text{C}$ (nm)	$^{19}\text{F}$ (nm)
35	1.92	17.16	34.32	78.72	12.99	10.37
40	1.08	13.36	26.72	44.88	7.87	6.92
45	0.61	10.39	20.78	25.39	4.93	4.94
50	0.34	8.05	16.10	14.38	3.27	3.82
55	0.19	6.20	12.40	8.14	2.32	3.18
60	0.10	4.73	9.46	4.59	1.79	2.82

TABLE I: The critical energy  $E_c$ , critical radius  $R_c$ , and critical diameter  $2R_c$  for bubble nucleation in superheated liquid  $\text{Zn}$  at a pressure of 1 atm and various operating temperatures. The values of the range,  $R(E = E_c)$ , of  $^1\text{H}$ ,  $^{12}\text{C}$  and  $^{19}\text{F}$  nuclei of energy  $E_c$  in liquid  $\text{Zn}$  at different temperatures are also listed for easy comparison with the values of  $2R_c$  at the corresponding temperatures.

The values of  $E_c$  and  $2R_c$  are listed in Table I for various operating temperatures ranging from 35° C to 60° C. The ranges ( $R$ ) of  $^1\text{H}$ ,  $^{12}\text{C}$  and  $^{19}\text{F}$  nuclei of energy  $E_c$  in liquid  $\text{Zn}$  at different operating temperatures are also listed in Table I for easy comparison with the values of critical diameter  $2R_c$  at the corresponding temperatures.

To aid visualization, we display in Figure 1 the ranges of  $^1\text{H}$ ,  $^{12}\text{C}$  and  $^{19}\text{F}$  nuclei as functions of their energy and their comparison with the critical diameter  $2R_c$  at three different temperatures, namely, 35°, 45° and 55° C.

It is seen that the ranges of  $^{12}\text{C}$  and  $^{19}\text{F}$  at energy  $E_c$  at all temperatures of our interest are less than the corresponding critical diameter  $2R_c$ . Thus, within the Seitz model, the threshold energies of these nuclei in the case of  $\eta_T = 100\%$  are the same and equal to the Seitz threshold  $E_c$  at the corresponding temperature. For the case of  $\eta_T = 50\%$ , for example, the ranges of  $^{12}\text{C}$  and  $^{19}\text{F}$  at the energy  $2E_c$  at all temperatures under consideration are also less than  $2R_c$ , thus giving their bubble nucleation thresholds to be  $2E_c$ , as expected, since in this case only 50% of the total deposited energy goes into bubble nucleation. This behavior

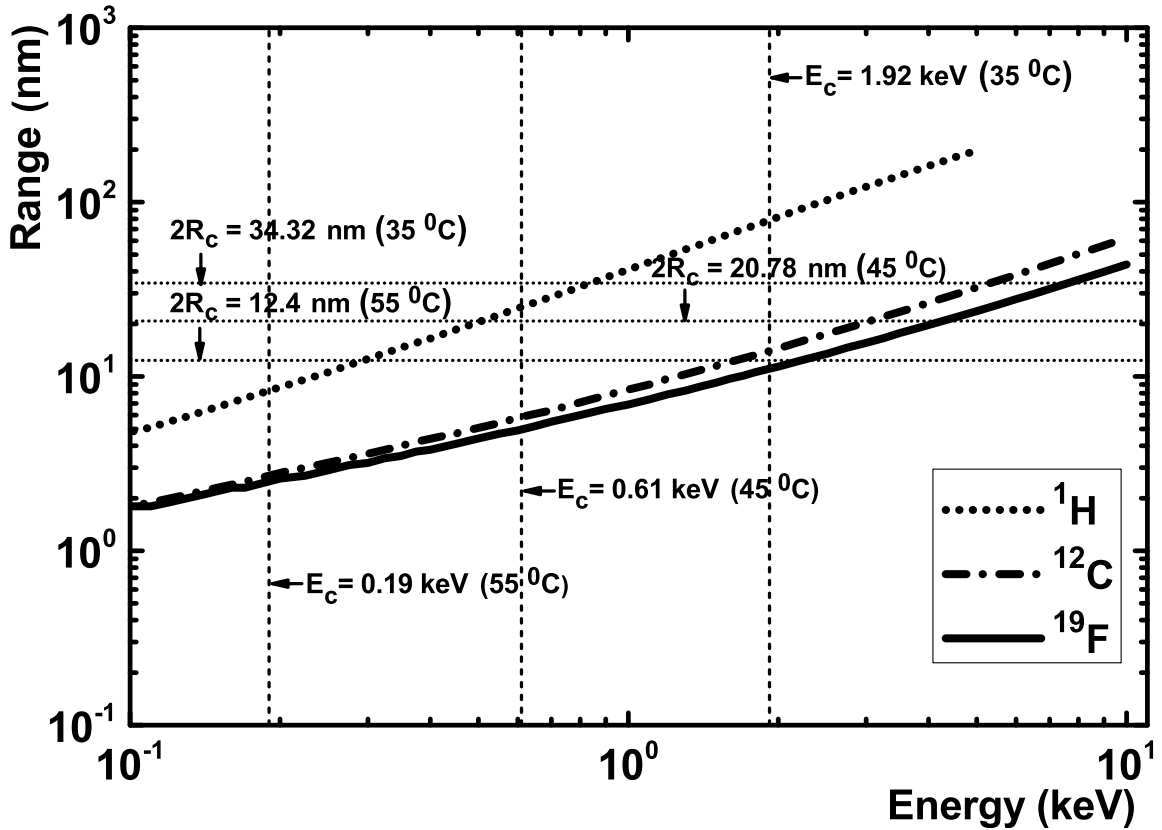


FIG. 1: Ranges of  $^1\text{H}$ ,  $^{12}\text{C}$  and  $^{19}\text{F}$  nuclei in superheated liquid water as functions of their energy. The dashed vertical lines mark the critical energy  $E_c$  at three different temperatures, namely,  $35^\circ$ ,  $45^\circ$  and  $55^\circ\text{C}$ , and the dotted horizontal lines mark the corresponding values of  $2R_c$ .

of nucleation thresholds of  $^{12}\text{C}$  and  $^{19}\text{F}$  being set at  $E_c(T)/\eta_T$  (owing to validity of the condition  $R(E_c(T)/\eta_T) \leq 2R_c(T)$ ) remains true for lower values of  $\eta_T$  too, but only at progressively higher temperatures as the value of  $\eta_T$  is decreased.

The case of  $^1\text{H}$  is, however, very different. The range of  $^1\text{H}$  at  $E_c$  is larger than  $2R_c$  at all temperatures below  $\sim 50^\circ\text{C}$ . Thus, even in the case of  $\eta_T = 100\%$ , the bubble nucleation threshold energy of  $^1\text{H}$  at temperatures below  $\sim 50^\circ\text{C}$  will be larger than  $E_c$  at the corresponding temperatures and will have to be determined by finding the energy at which equation (2) is satisfied. This is illustrated in Figure 2 for  $\eta_T = 100\%$  and  $50\%$ . The resulting threshold energies of  $^1\text{H}$ ,  $^{12}\text{C}$  and  $^{19}\text{F}$  as functions of temperature are shown graphically in Figure 3 for the two cases of  $\eta_T = 100\%$  and  $50\%$ .

With the threshold energies of  $^1\text{H}$ ,  $^{12}\text{C}$  and  $^{19}\text{F}$  determined as above, we can calculate

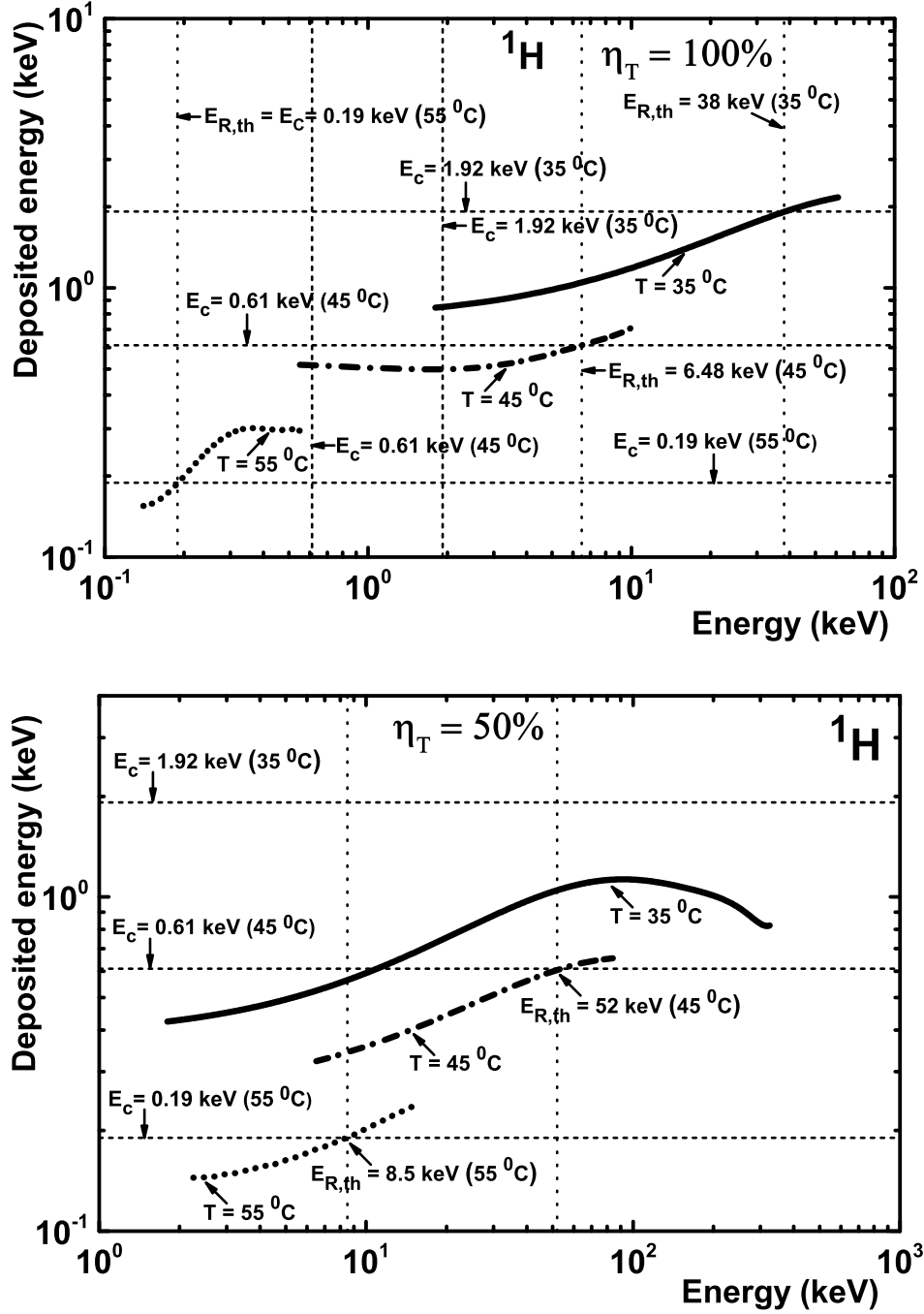


FIG. 2: Energy deposited by  $^1\text{H}$  nuclei over the length scale  $2R_c$  in superheated liquid  $2\text{h}2\text{f}4$  for temperatures  $35^\circ$ ,  $45^\circ$  and  $55^\circ\text{C}$  for  $\eta_T = 100\%$  (upper panel) and  $\eta_T = 50\%$  (lower panel). The vertical and horizontal dashed lines mark the values of the critical energy  $E_c$  at different temperatures. The  $^1\text{H}$  threshold energies ( $E_{R,th}$ ) obtained from crossings of the energy deposition curves with the horizontal  $E_c$  lines for the three different temperatures are marked by vertical dotted lines. Note that for  $55^\circ\text{C}$ ,  $E_{R,th}$  and  $E_c$  coincide in the case of  $\eta_T = 100\%$ . Also, for  $T = 35^\circ\text{C}$ , there is no solution of equation (2) for the case of  $\eta_T = 50\%$ .

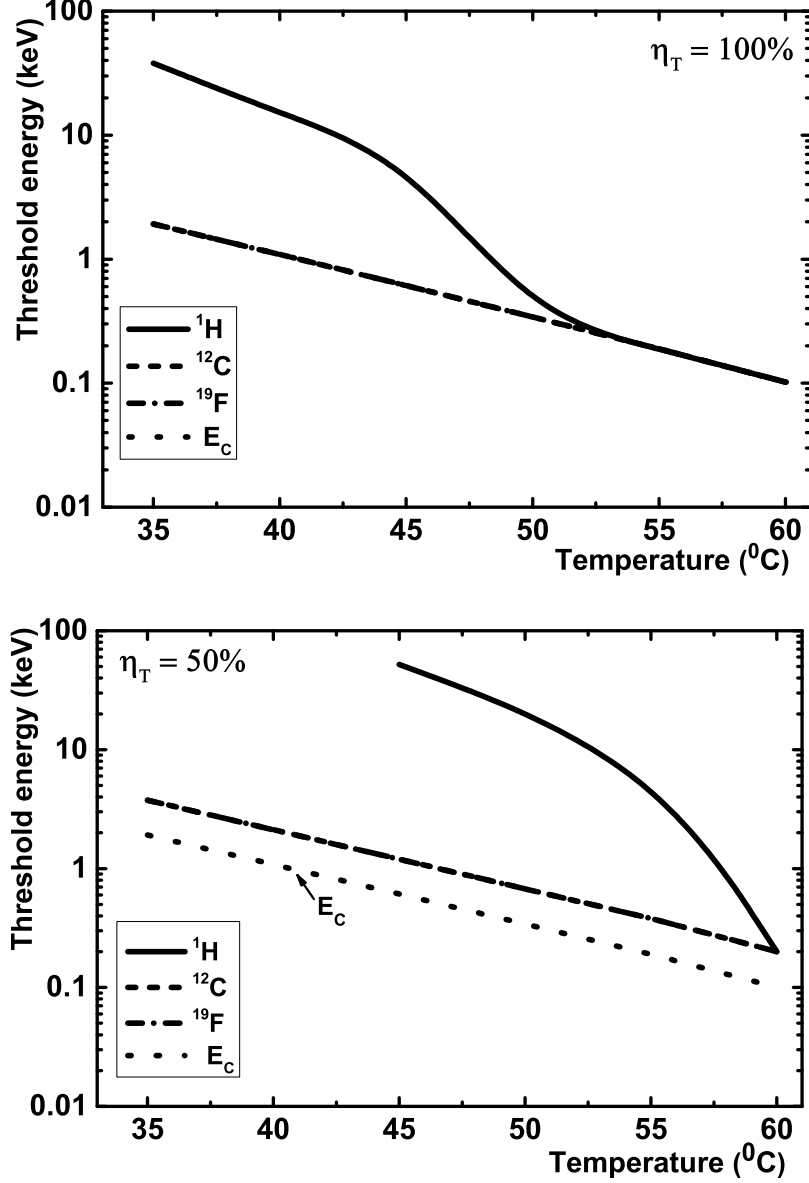


FIG. 3: The threshold energy for bubble nucleation by recoiling  $^1\text{H}$ ,  $^{12}\text{C}$  and  $^{19}\text{F}$  for the case  $\eta_T = 100\%$  (upper panel) and  $\eta_T = 50\%$  (lower panel) in superheated liquid  $\text{Zn}$  as functions of temperature. Note that the thresholds of  $^{12}\text{C}$  and  $^{19}\text{F}$  coincide with  $E_c(T)$  for  $\eta_T = 100\%$ , and with  $2E_c(T)$  for the case  $\eta_T = 50\%$ .

the temperature dependence of the lowest WIMP mass to which superheated liquid  $\text{Zn}$  can be sensitive for different values of  $\eta_T$ , using equation (15). The results are displayed in Table II and shown graphically in Figure 4.

From Table II and Figure 4, we see that, with suitable choice of the operating temperature,

T (° C)	$(\eta_T = 25\%)$						$(\eta_T = 50\%)$						$(\eta_T = 100\%)$					
	$E_{R,\text{th}}$ (keV)			$m_{\chi,\text{lowest}}$ (GeV)			$E_{R,\text{th}}$ (keV)			$m_{\chi,\text{lowest}}$ (GeV)			$E_{R,\text{th}}$ (keV)			$m_{\chi,\text{lowest}}$ (GeV)		
	$^1\text{H}$	$^{12}\text{C}$	$^{19}\text{F}$	$^1\text{H}$	$^{12}\text{C}$	$^{19}\text{F}$	$^1\text{H}$	$^{12}\text{C}$	$^{19}\text{F}$	$^1\text{H}$	$^{12}\text{C}$	$^{19}\text{F}$	$^1\text{H}$	$^{12}\text{C}$	$^{19}\text{F}$	$^1\text{H}$	$^{12}\text{C}$	$^{19}\text{F}$
35	-	250.0	8.0	-	-	6.34	-	3.84	3.84	-	3.29	3.90	38.0	1.92	1.92	-	2.17	2.63
40	-	22.0	4.32	-	13.69	4.25	-	2.16	2.16	-	2.36	2.84	15.16	1.08	1.08	-	1.55	1.90
45	-	2.44	2.44	-	2.54	3.06	52.0	1.22	1.22	-	1.65	2.01	6.48	0.61	0.61	-	1.13	1.39
50	-	1.36	1.36	-	1.77	2.16	20.0	0.68	0.68	-	1.20	1.48	0.34	0.34	0.34	0.29	0.82	1.02
55	55.0	0.76	0.76	-	1.31	1.61	8.50	0.38	0.38	-	0.87	1.08	0.19	0.19	0.19	0.20	0.60	0.75
60	22.50	0.40	0.40	-	0.89	1.11	0.20	0.20	0.20	0.21	0.62	0.77	0.10	0.10	0.10	0.14	0.43	0.54

TABLE II: Threshold energies of WIMP-induced recoiling  $^1\text{H}$ ,  $^{12}\text{C}$  and  $^{19}\text{F}$  nuclei for bubble nucleation in superheated liquid  $\text{ZnHf}_4$  at different temperatures for  $\eta_T = 25\%$ ,  $\eta_T = 50\%$  and  $\eta_T = 100\%$  and the corresponding lowest values of the WIMP mass that can produce those recoil nuclei of the respective threshold energies, i.e., the lowest mass WIMPs that can be probed with a  $\text{ZnHf}_4$  superheated liquid detector. A blank (-) entry indicates no sensitivity to the target element at the temperature under consideration, i.e.,  $E_{R,\text{th}}^{(i)}(T) > E_{R,\text{max}}^{(i)}$  for the target element  $i$ .

a  $\text{ZnHf}_4$  SLD can serve as a good detector for very low mass (sub-GeV – few GeV) WIMPs. In a separate experimental work [30] it is shown that at temperatures  $T < (38.5 \pm 1.4)^\circ\text{C}$ ,  $\text{ZnHf}_4$  is insensitive to gamma rays (which can cause nucleation events through electron recoils), though sensitive to neutrons (which give nucleation events through nuclear recoils). Thus, a sufficiently large  $\text{ZnHf}_4$  SLD operated at  $T \sim 35^\circ\text{C}$ , for example, would be sensitive to WIMP-induced  $^{12}\text{C}$  recoil events for WIMPs of mass in the few GeV range down to  $\sim 2.2$  GeV in the case of  $\eta_T = 100\%$  and  $\sim 3.3$  GeV in the case of  $\eta_T = 50\%$  without being sensitive to background  $\gamma$ -rays. However, for sub-GeV mass WIMPs, the SLD would need to be operated at higher temperatures. From Table II and Figure 4, we see that, the presence of hydrogen in  $\text{ZnHf}_4$  can make the SLD sensitive to WIMPs of mass down to  $\lesssim 200$  MeV at temperatures  $T \gtrsim 60^\circ\text{C}$  for  $\eta_T \geq 50\%$ . However, at these temperatures the  $\text{ZnHf}_4$  SLD becomes sensitive to background  $\gamma$ -rays as well.

Note from equation (15) that for a given recoiling nucleus  $i$ ,  $m_{\chi,\text{lowest}}^{(i)}$  roughly scales as  $(E_{R,\text{th}}^{(i)})^{1/2}$  for  $E_{R,\text{th}}^{(i)} \ll 2m_{A_i}v_{\text{esc}}^2$ . Thus, for  $^{12}\text{C}$  and  $^{19}\text{F}$ , an upward shift of the bubble

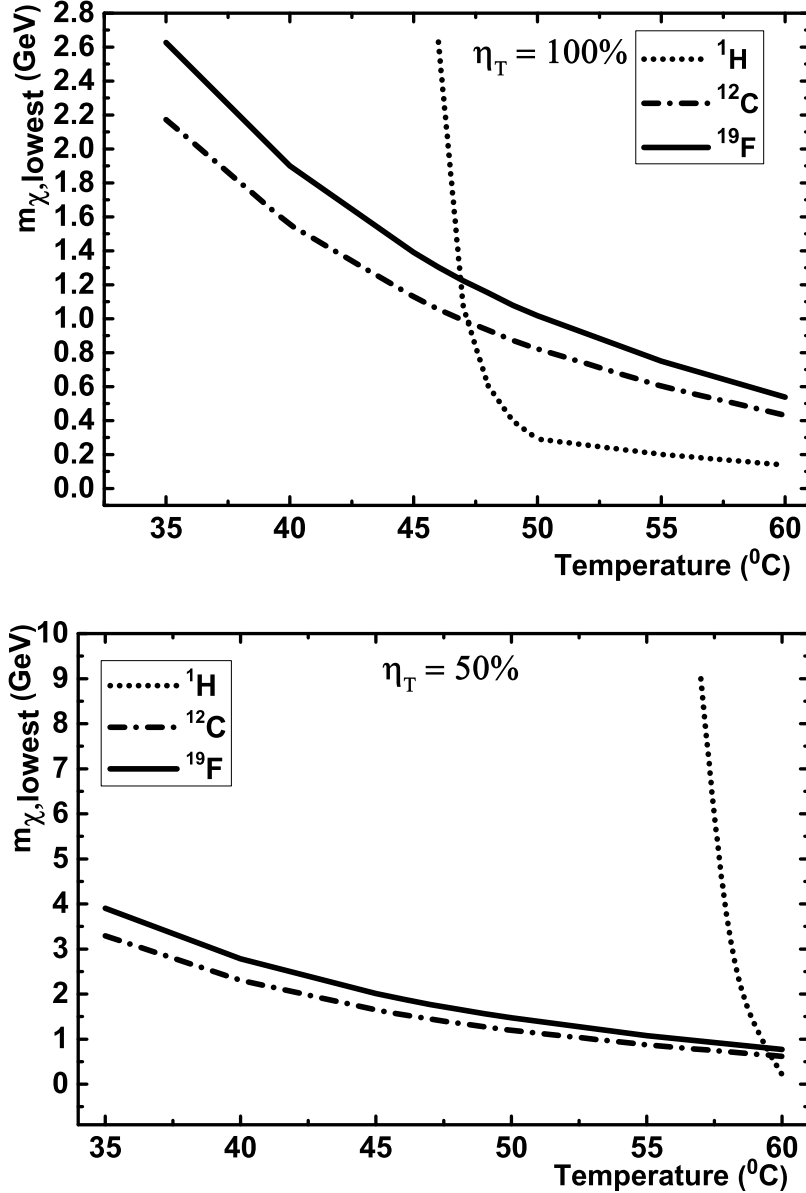


FIG. 4: Lowest WIMP masses that can produce recoiling  $^1\text{H}$ ,  $^{12}\text{C}$  and  $^{19}\text{F}$  nuclei above their bubble nucleation threshold energies (see Table II) in superheated liquid  $2\text{h}2\text{f}4$  as a function of temperature, for  $\eta_T = 100\%$  (top panel) and  $\eta_T = 50\%$  (bottom panel).

nucleation threshold energy from the Seitz threshold  $E_c$  by a factor of 2 (as is the case for  $^{12}\text{C}$  and  $^{19}\text{F}$  when  $\eta_T$  changes from 100% to 50%), for example, shifts the corresponding  $m_{\chi,\text{lowest}}$  upwards by a factor roughly between 1.4 and 1.5. So, as far as probing the few-GeV WIMP-mass region with  $^{12}\text{C}$  and  $^{19}\text{F}$  recoils in  $2\text{h}2\text{f}4$  is concerned, we do not expect substantial changes in our results for the WIMP-mass sensitivity of  $2\text{h}2\text{f}4$  estimated assuming

the relevant thresholds fixed at the respective Seitz thresholds  $E_c$  (i.e., assuming  $\eta_T = 100\%$ ) unless the actual threshold energies of these nuclei are larger than their Seitz thresholds by factors substantially larger than 2 (i.e.,  $\eta_T \ll 50\%$ ).

## B. Recoil spectra and event rates for low mass WIMPs

The low WIMP-mass sensitivity of a  $\mathcal{Z}h2f4$  SLD can be seen more clearly by looking at the expected contributions of  $^1\text{H}$ ,  $^{12}\text{C}$  and  $^{19}\text{F}$  nuclei to the rate of WIMP-induced nuclear recoil events. For this purpose, we calculate the differential recoil spectra of  $^1\text{H}$ ,  $^{12}\text{C}$  and  $^{19}\text{F}$  nuclei in  $\mathcal{Z}h2f4$  from equation (9) for a benchmark value of  $\sigma_{\chi n}^{\text{SI}} = 1 \text{ pb}$  — these are shown in Figure 5 — and then integrate these spectra (see equation (13)) over the recoil energies to obtain the rates as a function of WIMP mass at various temperatures using the corresponding threshold energies listed in Table II.

Following the discussions in section II, we take the bubble nucleation efficiencies,  $\epsilon_i(E_R)$ , in equation (13) for the recoiling  $^{12}\text{C}$  and  $^{19}\text{F}$  nuclei in  $\mathcal{Z}h2f4$  to be the same as the respective efficiencies for these nuclei in the liquid  $\text{C}_3\text{F}_8$  determined by the PICO experiment [36]. The piecewise linear function fits to the best-fit efficiency curves for  $^{12}\text{C}$  and  $^{19}\text{F}$  taken from the respective curves in the upper and lower panels of Figure 3 of Ref. [36] are shown in Figure 6. We see some small differences in the shapes of the efficiency curves for  $^{12}\text{C}$  obtained from the upper and lower panels of Figure 3 of Ref. [36] (which correspond to the solid and dashed curves, respectively, in our Figure 6), while the two curves for  $^{19}\text{F}$  are essentially identical. We verify that these differences between the solid and dashed curves for  $^{12}\text{C}$  in Figure 6 do not make any significant difference in our results for the event rates and WIMP-mass sensitivities presented below. For definiteness, below we shall use the efficiency curves for  $^{12}\text{C}$  and  $^{19}\text{F}$  recoils represented by the solid curves in the upper and lower panels, respectively, of Figure 6, for calculating the event rates and WIMP-mass sensitivities due to  $^{12}\text{C}$  and  $^{19}\text{F}$  recoils in  $\mathcal{Z}h2f4$ . For  $^1\text{H}$  recoils, as already mentioned, we shall use a step-function efficiency curve at the relevant bubble nucleation threshold for  $^1\text{H}$ .

The resulting rates (in units of  $\text{kg}^{-1} \text{ day}^{-1}$ ) as a function of WIMP mass for two different temperatures,  $T = 35^\circ \text{C}$  and  $T = 55^\circ \text{C}$ , for the case of  $\eta_T = 100\%$ , are shown in Figure 7 and those for the case of  $\eta_T = 50\%$  are shown in Figure 8.

The event rates shown in these Figures scale linearly with the value of  $\sigma_{\chi n}^{\text{SI}}$ , and the

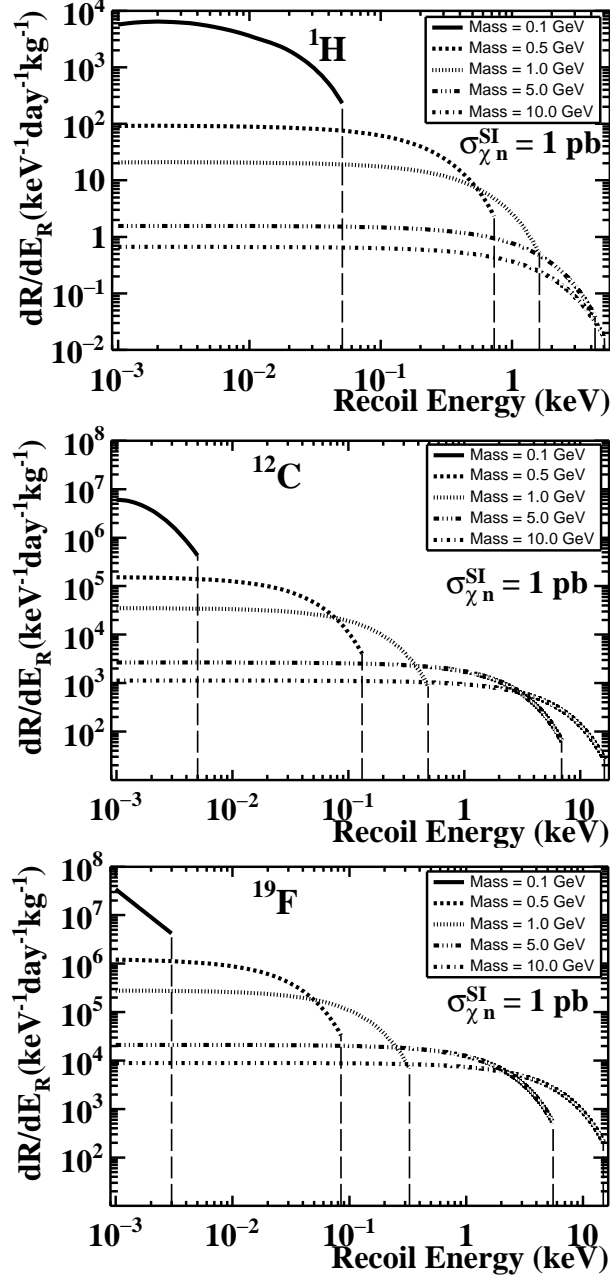


FIG. 5: Differential recoil energy spectra, as given by equation (9), of  ${}^1\text{H}$ ,  ${}^{12}\text{C}$  and  ${}^{19}\text{F}$  nuclei in  $\text{Zh}2\text{f}4$  (per keV of recoil energy per day per kg of  $\text{Zh}2\text{f}4$ ) for different WIMP masses for a benchmark value of the WIMP-nucleon spin-independent (SI) cross section,  $\sigma_{\chi n}^{\text{SI}} = 1 \text{ pb} (= 10^{-36} \text{ cm}^2)$ . (Note: One kg of  $\text{Zh}2\text{f}4$  contains 0.02 kg of  ${}^1\text{H}$ , 0.235 kg of  ${}^{12}\text{C}$  and 0.745 kg of  ${}^{19}\text{F}$ .) Other parameter values used are:  $\rho_{\text{DM}} = 0.3 \text{ GeV}/\text{cm}^3$ ,  $v_0 = 220 \text{ km s}^{-1}$ ,  $v_E = 232 \text{ km s}^{-1}$  and  $v_{\text{esc}} = 540 \text{ km s}^{-1}$ . The dashed vertical lines mark the sharp cutoff of the recoil spectra due to the sharp cutoff of the speed distribution of the WIMPs at the escape velocity  $v_{\text{esc}}$  (see text).

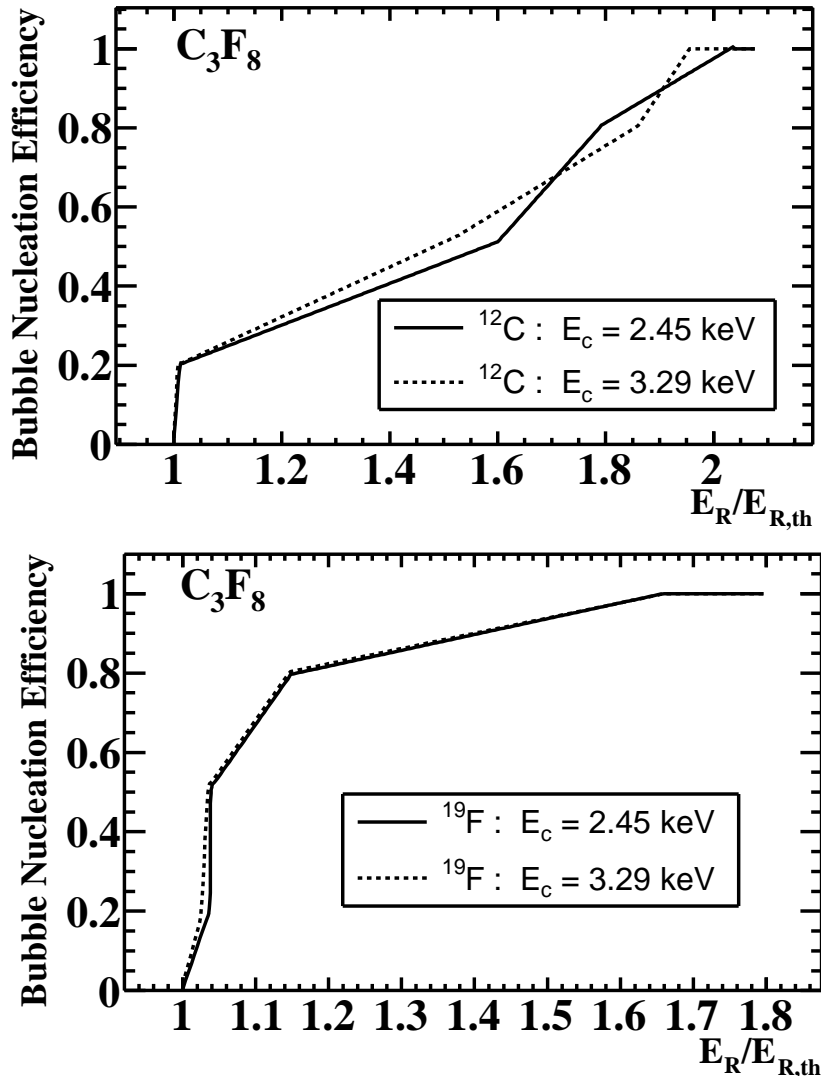


FIG. 6: Piecewise linear function fits to the best-fit bubble nucleation efficiency curves for  $^{12}C$  (upper panel) and  $^{19}F$  (lower panel) recoils in  $C_3F_8$  taken from Figure 3 of Ref. [36]. In each case, the curves reconstructed from the upper as well as lower panels of Figure 3 of Ref. [36] corresponding to two different values of the Seitz thresholds  $E_c=2.45$  (solid curves) and 3.29 keV (dashed curves) in  $C_3F_8$ , respectively, are shown for comparison.

number of events scale with the total exposure (kg.day). The WIMP-mass thresholds for contributions of different nuclei to the total event rates directly reflect the lowest WIMP-mass sensitivities shown in Table II and Figure 4.

From Figures 7 and 8 we see that in the few GeV WIMP mass region the total event rates are generally dominated by contributions from recoiling  $^{12}C$  and  $^{19}F$  nuclei. The

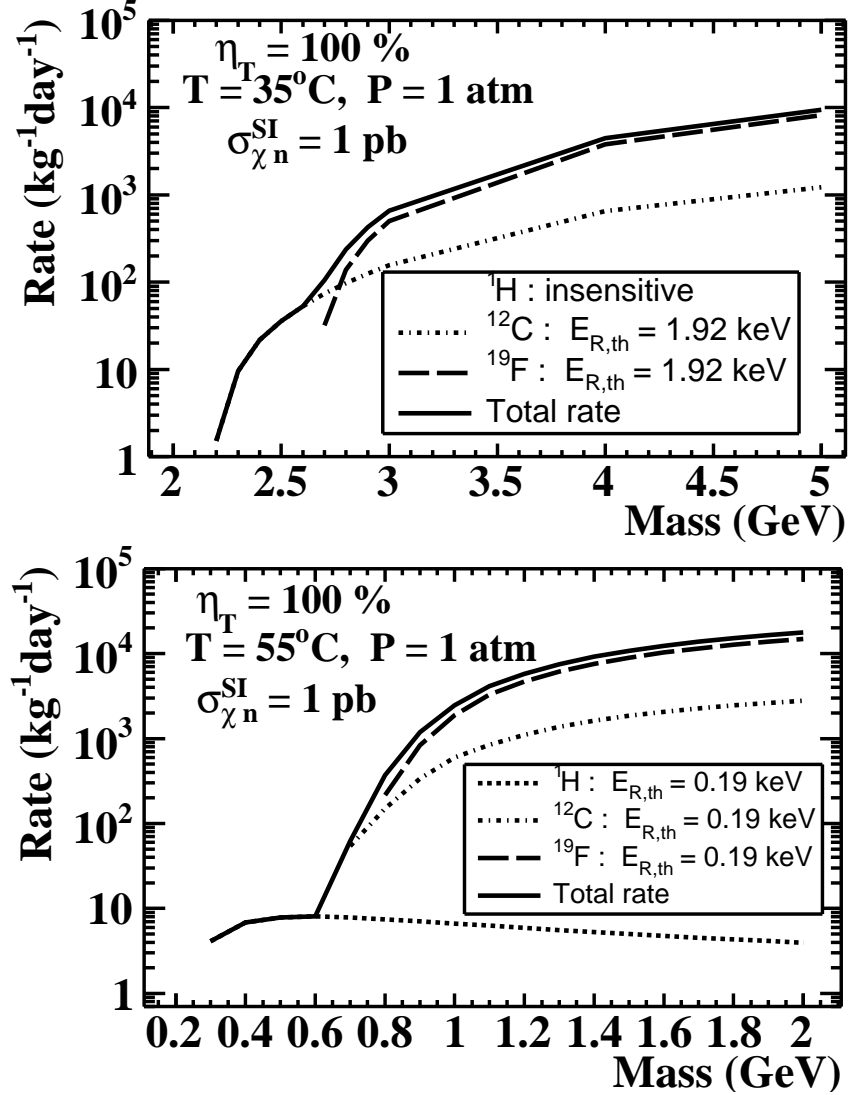


FIG. 7: Contributions of  $^1\text{H}$ ,  $^{12}\text{C}$  and  $^{19}\text{F}$  to the total rate of WIMP-induced nuclear recoil events in a  $\text{ZnF}_2$  SLD operated at a temperature of  $35^\circ\text{C}$  (upper panel) and  $55^\circ\text{C}$  (lower panel) and pressure of 1 atm, as a function of the WIMP mass ( $\lesssim$  few GeV) for a benchmark value of spin-independent WIMP-nucleon cross section,  $\sigma_{\chi n}^{\text{SI}} = 1\text{ pb}$ , for the case of  $\eta_T = 100\%$ . The bubble nucleation thresholds of individual nuclei used in the calculation are as listed in Table II). Note that, at  $T = 35^\circ\text{C}$ , the WIMP-induced recoiling  $^1\text{H}$  nuclei do not contribute any event since their maximum possible recoil energies (see Figure 5) are below their bubble-nucleation threshold energy at this temperature; see Figure 3 and Table II. The sharp fall-off of the rates for different nuclear species at the lower mass end reflects the lowest WIMP mass sensitivities of the different nuclei shown in Table II and Figure 4.

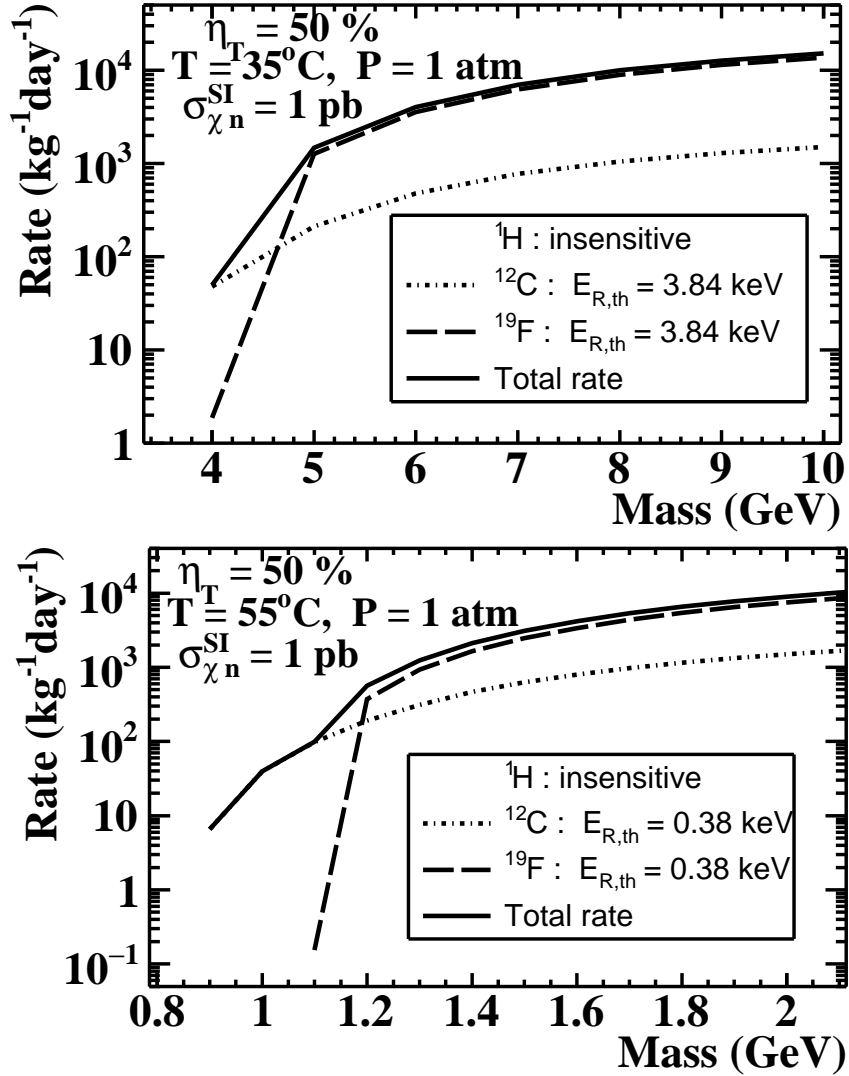


FIG. 8: Same as Figure 7 but for  $\eta_T = 50\%$ . Note that in this case there is no sensitivity to  $^1\text{H}$  at both  $35^\circ\text{C}$  and  $55^\circ\text{C}$  — the  $^1\text{H}$  sensitivity appears only at  $T \gtrsim 60^\circ\text{C}$  in the case of  $\eta_T = 50\%$ ; see Table II.

sub-GeV WIMP mass region can be probed only by operating the detector at relatively high temperatures of  $T \gtrsim 55^\circ\text{C}$ . At such high temperatures, however, the detector will be sensitive to background gamma rays [30], which would give rise to bubble nucleation events through electron recoils (ER). This would seriously limit the potential of a  $\text{ZnF}_2$  detector for probing sub-GeV mass WIMPs unless effective means of rejection of the ER background can be found.

In this context, recent work by the PICO collaboration [43] on electron recoils in  $\text{C}_3\text{F}_8$  may

point to a possible way forward. The analysis of gamma calibration data on  $\text{C}_3\text{F}_8$  in Ref. [43] showed that bubble nucleation due to electron recoils in  $\text{C}_3\text{F}_8$  is better described in terms of a new nucleation mechanism that is driven by ionization through  $\delta$ -electron production rather than by localized energy deposition envisaged in the standard Seitz heat spike model that well describes nucleation caused by nuclear recoils. Consequently, bubble nucleation thresholds for electron and nuclear recoils scale differently with the thermodynamic operating conditions of the detector. In particular, the analysis of Ref. [43] suggests that it may be possible to minimize the nuclear recoil bubble nucleation threshold while maximizing the ER nucleation threshold by operating the detector at the lowest possible pressure. The operating temperature can then be tuned to the desired (low) nuclear recoil threshold, thereby making the detector largely insensitive to electron recoils without losing sensitivity to low energy nuclear recoil events. While it still remains to be demonstrated if this new model of ER bubble nucleation discussed in Ref. [43] for  $\text{C}_3\text{F}_8$  would also be valid for other light element liquids, in particular  $\text{ZnF}_4$ , the liquid of our interest in the present paper, below we estimate the level of sensitivity of a  $\text{ZnF}_4$  detector to low mass WIMPs under the assumption that appropriate thermodynamic operating conditions of the detector can be chosen so as to make such a detector insensitive to background gamma rays.

### C. Sensitivity of $\text{ZnF}_4$ detectors to low mass WIMPs under zero background assumption

Under the assumption of zero background, the standard Poissonian 90% C.L. upper limit on the WIMP-nucleon spin-independent cross section,  $\sigma_{\chi n,90}^{\text{SI}}$ , for zero observed number of events (which corresponds to a total of 2.3 expected number of events) is given by

$$\frac{\sigma_{\chi n,90}^{\text{SI}}}{1 \text{ pb}} \equiv \frac{2.3}{\mathcal{R}_{\text{exp}} \mathcal{E}}, \quad (16)$$

where  $\mathcal{E}$  is the total exposure (in units of kg.day), and the expected total event rate  $\mathcal{R}_{\text{exp}}$  is calculated in units of  $(\text{kg.day})^{-1}$  for  $\sigma_{\chi n}^{\text{SI}} = 1 \text{ pb}$  (see Figures 7 and 8).

Figure 9 shows  $\sigma_{\chi n,90}^{\text{SI}}$  as a function of WIMP mass (sub-GeV – few GeV) for a total exposure of  $\mathcal{E} = 10^3 \text{ kg.day}$  for  $\eta_{\text{T}} = 100\%$  and  $\eta_{\text{T}} = 50\%$ , in each case for two values of the operating temperature,  $T = 35^\circ \text{C}$  and  $55^\circ \text{C}$ .

It is seen that, in the situation of zero background, a  $\text{ZnF}_4$  SLD with  $\eta_{\text{T}} = 100\%$  operated

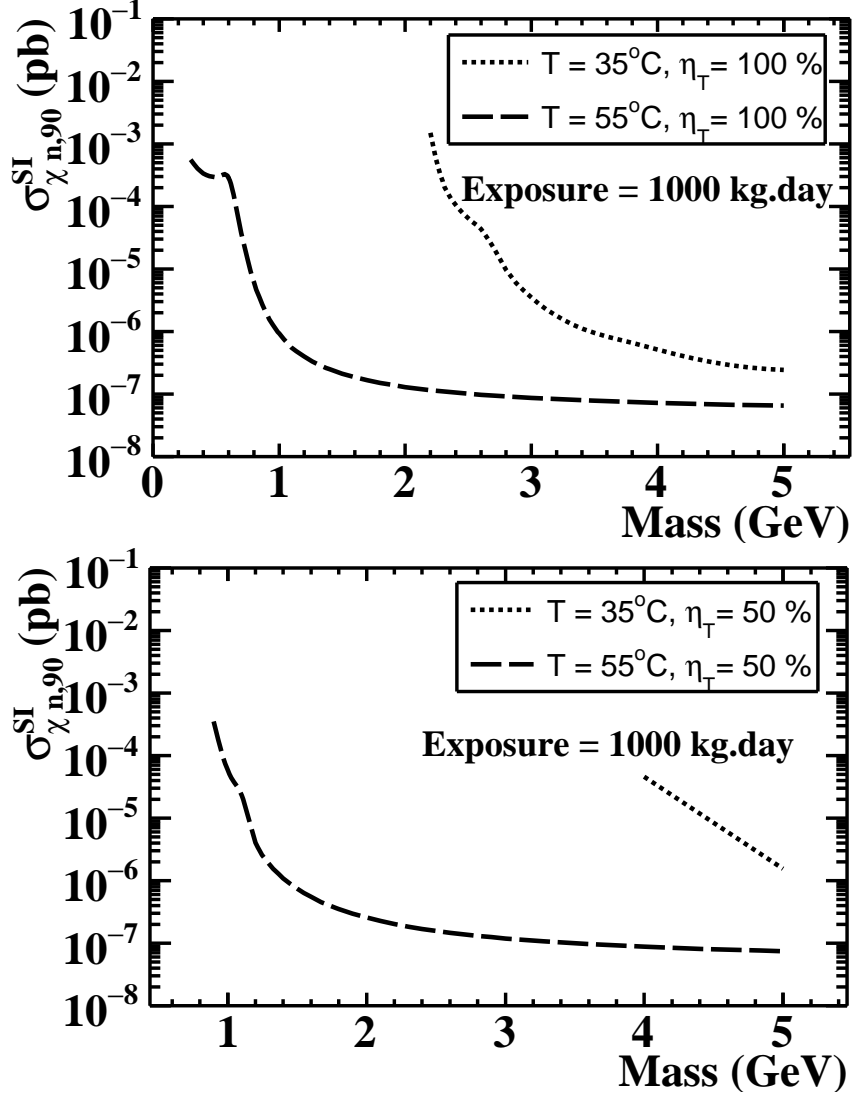


FIG. 9: 90% C.L. Poissonian upper limits on the spin-independent WIMP-nucleon cross section,  $\sigma_{\chi n, 90}^{SI}$ , as a function of WIMP mass for zero observed events under the assumption of zero background for a total exposure of 1000 kg.day, for operating temperatures  $T = 35^\circ\text{C}$  and  $55^\circ\text{C}$ , and  $\eta_T = 100\%$  (upper panel) and  $\eta_T = 50\%$  (lower panel).

at  $55^\circ\text{C}$  (corresponding to a Seitz threshold of 0.19 keV) with a total exposure of 1000 kg.day, for example, would be able to probe WIMPs of masses 5, 3, 2 and 1 GeV at the sensitivity levels of  $\sigma_{\chi n, 90}^{SI} = 6.5 \times 10^{-8}$ ,  $8.7 \times 10^{-8}$ ,  $1.3 \times 10^{-7}$  and  $9.3 \times 10^{-7}$  pb, respectively. Note that in the few-GeV mass region the event rates at  $55^\circ\text{C}$  are dominated by  $^{19}\text{F}$  recoils, with  $^{12}\text{C}$  recoils making sub-dominant and  $^1\text{H}$  recoils making negligible contributions. In the sub-GeV mass region, at  $55^\circ\text{C}$ , the sensitivities are at the levels of  $6.2 \times 10^{-6}$ ,  $3.7 \times 10^{-5}$ ,

$2.9 \times 10^{-4}$ , and  $5.6 \times 10^{-4}$  pb at  $m_\chi = 0.8, 0.7, 0.5$  and  $0.3$  GeV, respectively. Note that, at  $55^\circ\text{C}$ , the  $^{12}\text{C}$  and  $^{19}\text{F}$  recoils are unable to cause bubble nucleation events for WIMPs of masses  $\lesssim 0.6$  GeV, and the limits on  $\sigma_{\chi n}^{\text{SI}}$  for these WIMP masses come from WIMPs scattering on  $^1\text{H}$  only.

At the lower temperature of  $35^\circ\text{C}$ , again for  $\eta_{\text{T}} = 100\%$  (corresponding to a Seitz threshold of  $1.92$  keV), the sensitivities in the few GeV WIMP mass region worsen in comparison to those at  $55^\circ\text{C}$ , with  $\sigma_{\chi n,90}^{\text{SI}} = 2.5 \times 10^{-7}$ ,  $5.2 \times 10^{-7}$ ,  $3.5 \times 10^{-6}$  and  $2.2 \times 10^{-5}$  pb at  $m_\chi = 5, 4, 3$  and  $2.7$  GeV, respectively. Again, these limits come mainly from  $^{19}\text{F}$  recoils, with  $^{12}\text{C}$  recoils making sub-dominant and  $^1\text{H}$  recoils making no contribution. In the WIMP mass region  $2.2 \lesssim m_\chi \lesssim 2.6$  GeV, the  $^{12}\text{C}$  recoils make the dominant contribution to the event rate, giving a sensitivity at the level of  $\sim 1.5 \times 10^{-3}$  pb at  $m_\chi \sim 2.2$  GeV, the lowest WIMP mass that can be probed at  $35^\circ\text{C}$  in the case of  $\eta_{\text{T}} = 100\%$ .

In the case of  $\eta_{\text{T}} = 50\%$ , at  $T = 35^\circ\text{C}$ , in the few GeV WIMP-mass region, the  $\sigma_{\chi n,90}^{\text{SI}}$  sensitivities are at the levels of  $4.6 \times 10^{-5}$  pb and  $1.6 \times 10^{-6}$  pb at  $m_\chi = 4$  and  $5$  GeV, respectively. There is no sensitivity to sub-GeV WIMPs at this temperature. At the higher temperature of  $T = 55^\circ\text{C}$ , the sensitivities improve with reduction of thresholds, with values of  $7.5 \times 10^{-8}$ ,  $2.6 \times 10^{-7}$  and  $5.8 \times 10^{-5}$  pb at  $m_\chi = 5, 2$  and  $1$  GeV, respectively, for example, with dominant contributions to the event rates coming from  $^{19}\text{F}$  recoils for  $m_\chi = 5$  and  $2$  GeV, and from  $^{12}\text{C}$  recoils for  $m_\chi = 1$  GeV. There is only marginal sensitivity to sub-GeV mass WIMPs, which can be reached only at  $T \gtrsim 60^\circ\text{C}$  in this case of  $\eta_{\text{T}} = 50\%$ .

## V. SUMMARY AND CONCLUSIONS

In this paper we have theoretically studied the potential of a superheated liquid detector (SLD) with a hydrogen containing liquid, namely, tetrafluoroethane ( $\text{C}_2\text{H}_2\text{F}_4$ ) (b.p.  $-26.3^\circ\text{C}$ ), as the active target material for probing low (sub-GeV – few GeV) mass WIMP candidates of dark matter. In a  $\text{C}_2\text{H}_2\text{F}_4$  SLD the recoiling  $^1\text{H}$ ,  $^{12}\text{C}$  and  $^{19}\text{F}$  nuclei arising from elastic scattering of the Galactic WIMPs on these nuclei can give rise to detectable bubble nucleation events if the recoil energies are above certain threshold energies. The latter are determined by the ‘‘Seitz condition’’ that a fraction  $\eta_{\text{T}} < 1$  (called the ‘‘thermodynamic efficiency’’) of the energy deposited by a recoiling nucleus in the liquid over a length scale of  $2R_c$  (where  $R_c$  is a critical length) has to be greater than or equal to a certain critical energy

$E_c$ . Both  $R_c$  and  $E_c$  are characteristics of the liquid under consideration, and depend on the operating temperature and pressure of the superheated liquid, thus making the threshold energies dependent on temperature at a given operating pressure.

We have discussed the calculation of the bubble nucleation threshold energies of the WIMP-induced recoiling  $^1\text{H}$ ,  $^{12}\text{C}$  and  $^{19}\text{F}$  nuclei in  $\text{ZnF}_2$  using the Seitz condition for various values of the parameter  $\eta_T$ . Guided by the results from the PICO experiment [36] on the experimental ranges of possible values for the bubble nucleation threshold energies and the nucleation efficiencies above their respective thresholds for  $^{12}\text{C}$  and  $^{19}\text{F}$  recoils in  $\text{C}_3\text{F}_8$ , we have shown the results for the event rates and WIMP-mass sensitivities for  $\text{ZnF}_2$  for two possible representative different values of  $\eta_T$ , namely, 50% and 100%, for illustration. For  $^1\text{H}$  recoils in  $\text{ZnF}_2$ , in absence of any direct experimental results on their nucleation efficiency curves, we have assumed 100% bubble nucleation efficiency at threshold as in previous studies [32].

In general, the bubble nucleation threshold energies of all nuclei decrease with increasing temperature irrespective of the value of  $\eta_T$ . In the ideal case of  $\eta_T = 1$ , by operating the detector at a relatively high temperature of  $T = 60^\circ\text{C}$ , for example, nucleation thresholds of  $\sim 0.1\text{ keV}$  (same for  $^1\text{H}$ ,  $^{12}\text{C}$  and  $^{19}\text{F}$ ) can be reached, allowing sub-GeV WIMP masses down to  $\sim 140, 430$  and  $540\text{ MeV}$  (due to  $^1\text{H}$ ,  $^{12}\text{C}$  and  $^{19}\text{F}$  recoils, respectively) to be probed. At such high temperatures, however, the detector will be sensitive to background gamma rays [30]. At a lower temperature of  $35^\circ\text{C}$ , for example, where the detector is expected to be insensitive to gamma rays,  $^{12}\text{C}$  and  $^{19}\text{F}$  thresholds of  $\sim 2\text{ keV}$  would be possible, making the detector sensitive to WIMPs of masses down to  $\sim 2.2\text{ GeV}$ . However, sensitivity to  $^1\text{H}$  recoils would be lost at this temperature.

In a perhaps more realistic situation of  $\eta_T = 0.5$ , for example,  $^{12}\text{C}$  and  $^{19}\text{F}$  thresholds move up, for reasons explained in section IV A, by a factor of 2 compared to their values for the case of  $\eta_T = 1$  at all temperatures of interest considered here, with lowest sensitive WIMP-mass moving upwards by factors between  $\sim 1.4$  and  $1.5$  compared to the case of  $\eta_T = 1$ . Sensitivity to  $^1\text{H}$  recoils now appear only at temperatures  $T \gtrsim 60^\circ\text{C}$  where, again, the detector will be sensitive to background gamma rays.

From the above discussions we see that few-keV level recoil energy thresholds possible for bubble nucleation in  $\text{ZnF}_2$  SLDs by recoiling  $^{12}\text{C}$  and  $^{19}\text{F}$  nuclei in  $\text{ZnF}_2$  at gamma-ray insensitive temperature regions of  $T \lesssim 35^\circ\text{C}$ , for example, have the potential to allow WIMPs

in the few-GeV mass range to be probed at a WIMP-nucleon spin-independent cross section sensitivity (90% C.L.) levels better than  $\sim 4.6 \times 10^{-5}$  pb at WIMP masses down to  $\sim 4$  GeV with a total exposure of  $\sim 1000$  kg.day, provided that thermodynamic efficiency  $\eta_T$  that determines the bubble nucleation thresholds for the recoiling  $^1\text{H}$ ,  $^{12}\text{C}$  and  $^{19}\text{F}$  nuclei in  $\text{ZnF}_4$  is  $\sim 50\%$  or higher. On the other hand, sensitivity to sub-GeV WIMP masses generally requires the detector to be sensitive to the WIMP-induced  $^1\text{H}$  recoils, which in turn requires the detector to be operated at gamma sensitive temperatures  $T \gtrsim 50^\circ\text{C}$  and  $\eta_T$  substantially larger than 50%.

As discussed above, the sensitivity of a  $\text{ZnF}_4$  detector to background gamma rays at high temperatures (corresponding to low Seitz thresholds), from sources both external as well as intrinsic to the detector material, poses a serious challenge for probing sub-GeV WIMP masses unless effective means of making the detector insensitive to background gamma rays, which would cause bubble nucleation due to electron recoils, can be found. In this regard, a possible way forward may come from a recent work by the PICO collaboration [43] which, based on gamma calibration data for  $\text{C}_3\text{F}_8$ , suggests a different mechanism of electron recoil induced bubble nucleation in  $\text{C}_3\text{F}_8$  than that envisaged in the standard Seitz heat spike scenario of bubble nucleation due to nuclear recoils. If this new scenario of gamma induced bubble nucleation in  $\text{C}_3\text{F}_8$  can be demonstrated to be valid for other light element liquids, in particular  $\text{ZnF}_4$ , then following the prescription in Ref. [43] it may be possible to push the electron recoil bubble nucleation thresholds to relatively higher energies while simultaneously lowering the nuclear recoil bubble nucleation thresholds to relatively lower energies by appropriately choosing the operating pressure and temperature of the detector, thereby making the detector largely insensitive to ER events without losing sensitivity to low energy hydrogen recoil events. We wish to explore this possibility in a future work.

**Acknowledgments :** We thank members of the PICO collaboration, in particular, Alan Robinson, Ubi Wichoski and Viktor Zacek, for useful comments. We wish to thank an anonymous referee for making valuable comments on a previous version of the manuscript, which has resulted in major changes and what we believe is a substantially improved version of the manuscript. This work is supported by grants under the CAPP-II project funded by the Dept. of Atomic Energy (DAE), Govt. of India. One of us (PB) acknowledges support under a DAE Raja Ramanna Fellowship.

- 
- [1] G. Steigman and M.S. Turner, Nucl. Phys. **B 253**, 375 (1985).
- [2] G. Jungman and M. Kamionkowski and K. Griest, Phys. Rep. **267**, 195 (1996).
- [3] G. Bertone, D. Hooper, and J. Silk, Phys. Rep. **405**, 279 (2005).
- [4] L. Roszkowski, E.M. Sessolo, and S. Trojanowski, Rept. Prog. Phys. **81**, 066201 (2018) [arXiv:1707.06277].
- [5] M.W. Goodman and E. Witten, Phys. Rev. **D31**, 3059 (1985).
- [6] R.J. Gaitskell, Annu. Rev. Nucl. Part. Sci. **54**, 315359 (2004).
- [7] T. Marrodan Undagoitia and L. Rauch, J. Phys. G **43**, 013001 (2016) [arXiv:1509.08767].
- [8] R. Bernabei *et al.* (DAMA collaboration), Eur. Phys. J. **C56**, 333 (2008) [arXiv:0804.2741].
- [9] R. Bernabei *et al.* (DAMA/LIBRA collaboration), Eur. Phys. J. **C67**, 39 (2010) [arXiv:1002.1028].
- [10] R. Bernabei *et al.* (DAMA/LIBRA collaboration), Eur. Phys. J. **C73**, 2648 (2013) [arXiv:1308.5109].
- [11] A.K. Drukier, K. Freese, and D.N. Spergel, Phys. Rev. **D33**, 3495 (1986); K. Freese, J. Friedman, and A. Gould, Phys. Rev. **D37**, 3388 (1988).
- [12] K. Freese, M. Lisanti, and C. Savage, Rev. Mod. Phys. **85**, 1561 (2013) [arXiv:1209.3339]; S. Baum, K. Freese, and C. Kelso, Phys. Lett. B **789**, 262 (2019) [arXiv:1804.01231].
- [13] G. Angloher *et al.* (CRESST collaboration), Eur. Phys. J. **C76**, 25 (2016) [arXiv:1509.01515].
- [14] C. Amole *et al.* (PICO collaboration), Phys. Rev. Lett. **118**, 251301 (2017) [arXiv:1702.07666].
- [15] D. S. Akerib *et al.* (LUX collaboration), Phys. Rev. Lett. **118**, 251302 (2017) [arXiv:1705.03380].
- [16] E. Aprile *et al.* (XENON collaboration), Phys. Rev. Lett. **119**, 181301 (2017) [arXiv:1705.06655].
- [17] X. Cui *et al.* (PandaX-II collaboration), Phys. Rev. Lett. **119**, 181302 (2017) [arXiv:1708.06917].
- [18] R. Agnese *et al.* (SuperCDMS collaboration), Phys. Rev. D **97**, 022002 (2018) [arXiv:1707.01632].
- [19] H. Jiang *et al.* (CDEX collaboration), Phys. Rev. Lett. **120**, 241301 (2018) [arXiv:1802.09016].
- [20] P. Agnese *et al.* (DarkSide collaboration), Phys. Rev. Lett. **121**, 081307 (2018)

- [arXiv:1802.06994].
- [21] Q. Arnaud *et al.* (NEWS-G collaboration), *Astropart. Phys.* **97**, 54 (2018) [arXiv:1706.04934].
- [22] E. Behnke *et al.* (PICASSO collaboration), *Phys. Rev. Lett.* **106**, 021303 (2011).
- [23] M. Felizardo *et al.* (SIMPLE collaboration), *Phys. Rev. D* **89**, 072013 (2014).
- [24] E. Behnke *et al.* (PICASSO collaboration), *Astropart. Phys.* **90**, 85 (2017).
- [25] A. Antonicci *et al.* (MOSCAB collaboration), *Eur. Phys. J.* **C77**, 752 (2017) [arXiv:1708.00101].
- [26] V.P. Skirpov, *Metastable Liquids*, Wiley, New York, 1974.
- [27] F. d’Errico, *Nucl. Instr. Meth. Phys. B* **184**, 229 (2001).
- [28] M. Das *et al.*, *Pramana – J. Phys.* **75**, 675 (2010).
- [29] P.K. Mondal, R. Sarkar, and B.K. Chatterjee, *Appl. Rad. Iso.* **90**, 1 (2014).
- [30] S. Sahoo, S. Seth and M. Das, *Nucl. Instr. Meth. Phys. A* **931**, 44 (2019).
- [31] A. Plante, V. Zacek (on behalf of Montreal group), PICO internal presentation (2016).
- [32] F. Tardif, Direct detection of dark matter with the PICO Experiment and the PICO-0.1 calibration chamber, MSc. thesis, University of Montreal (2018).
- [33] F. Seitz, *The Physics of Fluids* **1**, 2 (1958).
- [34] R.E. Apfel, S.C. Roy, and Y.-C. Lo, *Phys. Rev. A* **31**, 3194 (1985).
- [35] C. Amole *et al.* (PICO Collaboration), *Phys. Rev. D* **93**, 052014 (2016).
- [36] C. Amole *et al.* (PICO Collaboration), *Phys. Rev. D* **100**, 022001 (2019) [arXiv:1902.04031].
- [37] J. Lewin and P. Smith, *Astropart. Phys.* **6**, 87 (1996).
- [38] J.I. Read, *J. Phys. G* **41**, 063101 (2014) [arXiv:1404.1938].
- [39] J. Binney and S. Tremaine, *Galactic Dynamics* (2nd Edition), Princeton University Press (2008).
- [40] M.C. Smith *et al.* *Mon. Not. Roy. Astron. Soc.* **379**, 755 (2007) [arXiv:astro-ph/0611671].
- [41] E.W. Lemmon, M.L. Huber, and M.O. McLinden, NIST Standard Reference Database 23: Reference Fluid Thermodynamic and Transport Properties-REFPROP, Version 9.0, National Institute of Standards and Technology, Standard Reference Data Program, Gaithersburg, MD, USA, 2010 [<http://www.nist.gov/srd/nist23.cfm>].
- [42] J.F. Zeigler *et al.*, <http://www.srim.org>
- [43] C. Amole *et al.* (PICO Collaboration), *Phys. Rev. D* **100**, 082006 (2019) [arXiv:1905.12522].